Scheraga, H. A. (1986) *Ann. N.Y. Acad. Sci. 485*, 124.
Sippl, M. J., Némethy, G., & Scheraga, H. A. (1984) *J. Phys. Chem. 79*, 2361.
Stanfield, R. L., Fieser, T. M., Lerner, R. A., & Wilson, I. A. (1990) *Science 248*, 712.
Stimson, E. R., Meinwald, Y. C., Montelione, G. T., & Scheraga, H. A. (1986) *Int. J. Pept. Protein Res. 27*, 569.
Stone, S. R., & Hofsteenge, J. (1986) *Biochemistry 25*, 4622.
Stone, S. R., Dennis, S., & Hofsteenge, J. (1989) *Biochemistry 28*, 6857.
Sukumaran, D. K., Clore, G. M., Preuss, A., Zarbock, J., & Gronenborn, A. M. (1987) *Biochemistry 26*, 333.
Tsiang, M., Lentz, S. R., Dittman, W. A., Wen, D., Scarpati, E. M., & Sadler, J. E. (1990) *Biochemistry 29*, 10602.
Verlet, L. (1967) *Phys. Rev. 159*, 98.
Vu, T.-K. H., Hung, D. T., Wheaton, V. I., & Coughlin, S. R. (1991) *Cell 64*, 1057.
Wagner, G., Neuhaus, D., Wörgötter, E., Vasak, M., Kagi, J. H. R., & Wüthrich, K. (1984) *J. Mol. Biol. 187*, 131.
Weiner, S. J., Kollman, P. A., Case, D. C., Singh, U. C., Ghio, C., Alagona, G., Profeta, S., Jr., & Weiner, P. (1984) *J. Am. Chem. Soc. 106*, 765.
Wright, P. E., Dyson, H. J., & Lerner, R. A. (1988) *Biochemistry 27*, 7167.
Yue, S.-Y., DiMaio, J., Szewczuk, Z., Purisima, E. O., Ni, F., & Konishi, Y. (1991) *Protein Eng.* (in press).

The Ca^{2+} Ion and Membrane Binding Structure of the Gla Domain of Ca-Prothrombin Fragment 1[†,‡]

M. Soriano-Garcia,[§,∥] Kaillathe Padmanabhan,[§] A. M. de Vos,[⊥] and A. Tulinsky*[,§]

Department of Chemistry, Michigan State University, East Lansing, Michigan 48824, and Department of Protein Engineering, Genentech, Incorporated, 460 San Bruno Boulevard, South San Francisco, California 94080

Received September 17, 1991; Revised Manuscript Received December 11, 1991

ABSTRACT: The structure of Ca-prothrombin fragment 1 (residues 1–156 prothrombin) has been solved and refined at 2.2-Å resolution by X-ray crystallographic methods. The first two-thirds of the Gla domain (residues 1–48) and two carbohydrate chains (~5 kDa) are disordered in crystals of apo-fragment 1. When crystals are grown in the presence of Ca^{2+} ions, the Gla domain exhibits a well-defined structure binding seven Ca^{2+} ions, but the carbohydrate is still disordered. Even so, the crystallographic *R* factor reduced to 0.171. The folding of the Gla domain is dominated by 9–10 turns of three different α-helices. These turns produce two internal carboxylate surfaces composed of Gla side chains. A polymeric array of five Ca^{2+} ions separated by about 4.0 Å intercalates between the carboxylate surfaces. The coordination of the Ca^{2+} ions with Gla carboxylate oxygen atoms and water molecules leads to distorted polyhedral arrangements with μ-oxo bridges in a highly complex array that most likely orchestrates the folding of the domain. The overall mode of interaction of the Ca^{2+} ions is new and different from any Ca^{2+} ion–protein interactions heretofore observed or described. The fluorescence quenching event observed upon Ca^{2+} ion binding is due to a disulfide–π-electron interaction that causes a 100° reorientation of Trp42 of the Gla domain. The Ca^{2+} ion interaction also affords the N-terminus protection from acetylation because the latter is buried in the folded structure and makes hydrogen-bonding salt bridges with Gla17, Gla21, and Gla27. The Gla domain and its trailing disulfide unit associate intimately and together give rise to a domain-like structure. Electrostatic potential calculations indicate that the Gla domain is very electronegative. Since most of the carboxylate oxygen atoms of Gla residues are involved in Ca^{2+} ion binding, leaving only a few for bridging Ca^{2+} ion–phospholipid interactions, the role of bridging Ca^{2+} ions might be generally unspecific, with Ca^{2+} ions simply intervening between the negative Gla domain and negative head groups of the membrane surface. The folding of the kringle structure in apo- and Ca-fragment 1 is essentially the same. However, the Ser36–Ala47 helix of the Gla domain pivots around Cys48, shifting by approximately 30°, and the helix encroaches on the kringle producing some concomitant changes. These might be related to the protection of carbohydrate carrying Asn101 from acetylation in the Ca-fragment 1 structure.

Prothrombin is one of several proenzymes of blood involved in coagulation that undergoes posttranslational modification of glutamic acid residues in the N-terminal 48 or so residues to Gla[1] via a vitamin K dependent carboxylase (others are factors VII, IX, and X and the proteins designated C, S, and Z). The Gla residues vary in total number from 9 to 12 (Tulinsky et al., 1988) of which the first 10 are highly conserved (Figure 1). The function of the N-terminal residues of these zymogens is binding to membrane in the presence of Ca^{2+} ion (Gitel et al., 1973; Nelsestuen et al., 1974; Stenflo et al., 1974; Bajaj et al., 1975). They also bind Mg^{2+}, Sr^{2+}, and other metal ions (Furie et al., 1976; Bajaj et al., 1976; Nelsestuen et al., 1976; Bloom & Mann, 1978). Except for Sr^{2+} ions, the conformational change accompanying binding

[†] This work was supported by NIH Grant HL 25942.
[‡] The coordinates of the Ca-fragment 1 structure have been deposited in the Brookhaven Protein Data Bank (access no. 1PF2).
* To whom correspondence should be addressed.
[§] Michigan State University.
[∥] Present address: Instituto de Quimica, UNAM, Delegacion Coyoacan, Mexico D.F. 04510.
[⊥] Genentech, Inc.

[1] Abbreviations: Gla, γ-carboxyglutamic acid; fragment 1, prothrombin residues 1–156; ISIR, iterative single isomorphous replacement; EGF, epidermal growth factor; ANS, 1-anilinonaphthalene-8-sulfonate; fragment 1·2, prothrombin residues 1–274.

0006-2960/92/0431-2554$03.00/0

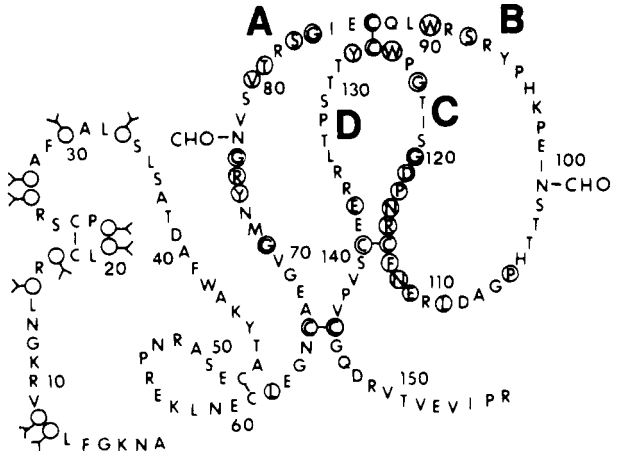

FIGURE 1: Sequence of prothrombin fragment 1. Gla domain (Ala1–Cys48); kringle domain (Cys66–Cys144); Gla residues, open circles; CHO, carbohydrate; residues conserved in kringle 2 of prothrombin are circled.

produces structures different from that induced by Ca^{2+} ion, some of which can, nonetheless, bind to phospholipid (Nelsestuen et al., 1976). The Ca^{2+} ion binding leads to intrinsic fluorescence quenching (Nelsestuen, 1976; Prendergast & Mann, 1977), and part of it is cooperative (Stenflo & Ganrot, 1973; Henriksen & Jackson, 1975; Nelsestuen et al., 1975; Bajaj et al., 1975; Deerfield et al., 1987) and appears to be crucial in forming the native conformation demanded by membrane binding. Further Ca^{2+} ion binding is thought to bridge carboxylate groups of Gla residues of the membrane binding structure and phosphate groups of a membrane surface (Nelsestuen, 1984). As a result of the autonomous nature of these Gla-containing N-terminal regions and their extraordinary high degree of homology (about two-thirds) (Tulinsky et al., 1988), they are commonly referred to as Gla domains.

The fluorescence, circular dichroism (Bloom & Mann, 1978), and other studies (Deerfield et al., 1987) have established two classes of metal ion binding sites in the Gla domain. The first class consists of about three relatively tight binding, higher affinity cooperative sites which are not metal ion specific, while the second 3–4 lower affinity sites (K_d = 0.65 mM) are specific for Ca^{2+} ions. Only strontium can satisfactorily replace calcium in both of these roles. A number of other cations can form protein structures that bind to phospholipid, but fluorescence measurements show that these are different from the one induced by Ca^{2+} ions (Nelsestuen et al., 1976), probably because of a different cooperativity of binding. Cations that bind to the high-affinity sites induce an intrinsic fluorescence quenching change (Nelsestuen et al., 1976; Prendergast & Mann, 1977), but only Sr^{2+} ion affects fluorescence and leads to phospholipid binding in a way comparable to Ca^{2+} ions. Two metal ion dependent transitions have been proposed to integrate all these observations on the basis of conformation-specific antibody studies (Borowski et al., 1986), where the first transition is not cation-specific while the second is selective for Ca^{2+} or Sr^{2+} ions and only the second transition produces the correct phospholipid-binding structure. However, since the binding of Mg^{2+} ion corresponds to that of five equivalent noninteracting sites that produces a fluorescence change but does not form a structure that binds to phospholipid, while Ca^{2+} ion binding displays three high-affinity cooperative sites (Deerfield et al., 1987), the conformational change reflected by the cooperative binding of the first few Ca^{2+} ions appears to be the one that leads to the essential membrane binding structure; the looser binding sites are probably more involved in charge neutralization and actual phospholipid binding (Nelsestuen et al., 1976, 1981; Bloom & Mann, 1978; Nelsestuen, 1984).

The structure of the Gla domain is disordered in bovine prothrombin fragment 1 (Park & Tulinsky, 1986; Tulinsky et al., 1988; Seshadri et al., 1991). The same is not the case when fragment 1 is crystallized in the presence of Ca^{2+} ions, which we reported and which possesses a definite structure at low resolution (2.8 Å) (Soriano-Garcia et al., 1989). However, because of small crystals, relatively limited X-ray diffraction data were available so that only a partial refinement of the structure was carried out (R_{final} = 0.31) and Ca^{2+} ions were not found. Subsequently, we have grown larger and much better X-ray diffraction quality crystals, which takes about one year, and a new and improved set of diffractometer intensity data was measured to high resolution (2.2 Å). We report here the highly refined structure of Ca-fragment 1 at 2.2-Å resolution. The positions of seven Ca^{2+} ions have been located in the Gla domain but required the revision of the folding of the peptide chain proposed earlier at lower resolution. The Ca^{2+} ion arrangement is polymeric, and the overall mode of interaction of the Ca^{2+} ions in the Gla domain is new and different from any Ca^{2+} ion–protein interactions heretofore observed or described [for a review see Strynadka and James (1989)].

Materials and Methods

Intensity Data Collection and Processing. Ca-prothrombin fragment 1 was crystallized as described earlier (Olsson et al., 1982; Soriano-Garcia et al., 1989). Crystals are orthorhombic, space group $P2_12_12_1$, cell dimensions a = 39.39 (1), b = 53.88 (4), and c = 129.64 (8) Å. One molecule of protein per asymmetric unit gives a crystal volume to protein mass ratio of 3.0 Å^3/dalton, which is in the range of values for crystals of proteins (Matthews, 1968) and corresponds to about 59% solvent. Large, freshly prepared crystals of Ca-fragment 1 diffract X-rays to 2.2-Å resolution with a sealed X-ray tube and would probably be a little better with high X-ray power.

A new and improved three-dimensional intensity data set was measured and processed at 2.2-Å resolution by using methods and procedures described in detail elsewhere (Tulinsky et al., 1973, 1985). One larger Ca-fragment 1 crystal having dimensions of 0.8 × 0.5 × 0.4 mm was employed, and a Nicolet P3/F four-circle diffractometer with a graphite monochrometer and Cu Kα radiation from a sealed X-ray tube operating at 2 kW of power were used. Reflections were measured by a wandering ω-step scan procedure (Wyckoff et al., 1967) consisting of seven 0.03° steps and taking the sum of the five largest contiguous counts as proportional to the integrated intensity. The decay and alignment of the crystal were monitored by repeatedly measuring the intensities of three strong reflections after every 100 measurements (~1 h). An intensity decrease in any of the monitor reflections of greater than 15% of the initially measured value triggered the recentering of a 13-reflection array and the calculation of a new orientation matrix. The intensity data were measured in four shells of decreasing 2θ (40–37.5°, 37.5–35°, 35–32°, and 32–2°) since intensities of higher Bragg angle reflections decay faster. A 6.0-Å resolution ($hk0$) data set was recorded before and after data collection for scaling purposes and for a lower Bragg angle intensity decay correction. Combining the information of the monitors, the 13-reflection array and the ratio between before and after data collection led to a 2θ-dependent decay correction with a maximum correction of 2.5 at 115 h of X-ray exposure; however, the maximum correction applied to a reflection was only 2.2 due to the sequential order of the data collection. Background measurements were averaged in

shells of 2θ, and average values were used to correct intensities. An empirical absorption correction was applied (North et al., 1968) (maximum correction of 1.57), and the intensity data were corrected for the Lorentz factor and polarization. Of 12 662 possible reflections at 2.2-Å resolution, 8141 (64%) were taken to be observed on the basis of a cutoff that was twice the absolute value of the average of the negative intensity measurements for a given 2θ range.

The mercury acetate heavy atom isomorphous derivative data of Ca-fragment 1 at 2.8-Å resolution collected previously (Soriano-Garcia et al., 1989) were used again here. It had been measured and processed employing similar methods and procedures to those just described. The derivative had two heavy atom sites with occupancies of 1.0 and 0.3 and was used in the present work in ISIR calculations with the new set of 2.2-Å resolution native data and proved to be critical for the determination of the structure of Ca-fragment 1.

Structure Solution and Refinement. Attempts to improve the original Ca-fragment 1 structure (Soriano-Garcia et al., 1989) by restrained least-squares refinement using the new diffraction data and $(2|F_o| - |F_c|)$ and $(|F_o| - |F_c|)$ electron density maps with various schemes for combining the phases from the molecular replacement model and those from solvent flattening ISIR procedures employing the mercury derivative proved to be sluggish and unsuccessful: R could only be decreased to 0.26–0.27, even when the data were restricted to only the 5.0–2.5-Å range with up to 40–50 water molecules included in the model structure. Since simulated annealing methods using the program XPLOR (Brunger et al., 1987) have a considerably larger radius of convergence, we subjected the structure to annealing between 3000 and 300 K with reflections satisfying $|F_o| > 4\sigma(|F_o|)$ in the 10.0–2.8-Å resolution range. The resulting R value of 0.26 for this range was encouraging, and the $(2|F_o| - |F_c|)$ electron density map and $(2|F_o| - |F_c|)$ omit maps (omitting various parts of the Gla domain especially between Cys18 and Leu32) suggested a new tracing of the polypeptide chain for residues Ser24–Gla30 which corresponded to two turns of α-helix between Arg25 and Ala31. Although the polypeptide chain density for this helix was clear, that of the adjoining conserved hexapeptide disulfide loop (Cys18–Cys23) and the remainder of the Gla domain was not and was broken in a number of places, still presenting ambiguities in connectivity, making difficult the interpretation of the chain path folding for the remaining residues. The situation was improved with the aid of a new set of phase combination calculations using the XPLOR phases and phases derived with the ISIR solvent flattening method with the mercury Ca-fragment 1 derivative (Wang, 1985). Six cycles of phase filtering were carried out, during which two separate molecular envelopes were calculated. The overall figure of merit improved from 0.50 to 0.89 with an accumulated phase shift of 66°. The phase-filtering procedure produced a marked improvement in the quality of the electron density map, which enabled the tracing of the Cys18–Cys23 disulfide loop of the Gla domain and presented possibilities for residues Ala1–Gla8 and Gla15–Gla17. A second simulated annealing using data in the 8.0–2.8-Å range was now carried out with a model including the disulfide loop, and the R factor decreased significantly to 0.23. The new XPLOR phases were again combined with ISIR solvent flattening calculations. Examination of the resulting $(2|F_o| - |F_c|)$ Fourier map showed the position of residues Val9–Leu14 and that the density of Leu14–Gla17 corresponded to a helical turn. In addition, four probable Ca^{2+} ion positions were also located. The assignment of the cations was based on large residual electron density in the difference map and on distances to Gla carboxylate ligands coordinated around them.

Table I: Summary of Final Restrained Least-Squares Parameters/Deviations and R Factor Statistics

	target	rms deviations
distances (Å)		
bond lengths	0.020	0.017
bond angles	0.040	0.055
planar 1–4	0.050	0.060
Ca–O	0.04	0.08
planes (Å)		
peptides	0.030	0.022
aromatic groups	0.030	0.033
chiral volumes (Å^3)	0.150	0.187
nonbonded contacts (Å)		
single torsion	0.60	0.24
multiple torsion	0.60	0.33
possible H-bond	0.60	0.34
thermal parameters (Å^2)		
main-chain bond	1.5	1.1
main-chain angle	2.0	1.8
side-chain bond	2.0	1.7
side-chain angle	2.5	2.5
torsion angles (deg)		
planar	3.0	3.1
staggered	15	26
orthonormal	20	18
diffraction pattern	*A*	*B*
$\sigma(\|F_o\|) = A + B[\sin\theta/\lambda - (1/6)]$	11	−100
$\langle\|\|F_o\| - \|F_c\|\|\rangle = 22$		
average angle = 117.5 ± 3.7°		

d_{min}	no. of reflections	$\sigma(\|F_o\|)$	$\langle\|\|F_o\| - \|F_c\|\|\rangle$	R factor shell	R factor sphere
4.60	854	18.4	35.4	0.168	0.168
3.80	969	15.6	28.9	0.142	0.155
3.30	1169	13.5	26.5	0.165	0.158
2.93	1153	11.6	21.6	0.179	0.162
2.65	1098	9.6	17.9	0.199	0.167
2.45	1023	8.0	14.4	0.193	0.169
2.20	1024	6.4	12.8	0.204	0.171

The refinement of this model was carried out using restrained least-squares methods with the programs PROLSQ (Hendrickson, 1985) and PROFFT (Finzel, 1987). The stereochemistry of the structure was restrained according to the weighting scheme shown in Table I. The refinement was performed in two stages, including data from 7.0–2.5-Å (58 cycles) and then 7.0–2.2-Å resolution (78 cycles), both with $|F_o| > \sigma(|F_o|)$. The refinement was interrupted by a number of interactive computer graphics sessions, during which the model was manually readjusted to fit the electron density along with inclusion of water solvent molecules. The Ca^{2+} ion–Gla residue interactions were fitted with the aid of electron and difference density maps to have Ca–O distances of about 2.4–2.6 Å. These were then used as ideal values, which were updated once to the refined values and were restrained during refinement. Since Ca–O distances to carboxylate groups range from 2.3 to 2.9 Å (Einspahr & Bugg, 1981), a looser restraint of 0.04 Å was applied (Table I) (comparable to angle–distance restraint). In the first refinement stage, the initial model consisted of 1149 atoms with 5821 reflections, and R decreased from 0.232 to 0.215. At the end of the stage, 61 solvent molecules had been located, and three more Ca^{2+} ions were identified. The final structure at 2.5-Å resolution with the water molecules and seven Ca^{2+} ions had an average R factor of 0.197. Refining the occupancies of the Ca^{2+} ions at this stage indicated that they were all essentially fully occupied.

The final stage of the refinement was carried out with 7290 reflections from 7.0–2.2-Å resolution. The solvent structure was increased by 84 water molecules in two additions, and a variable weighting scheme was applied to structure factors that

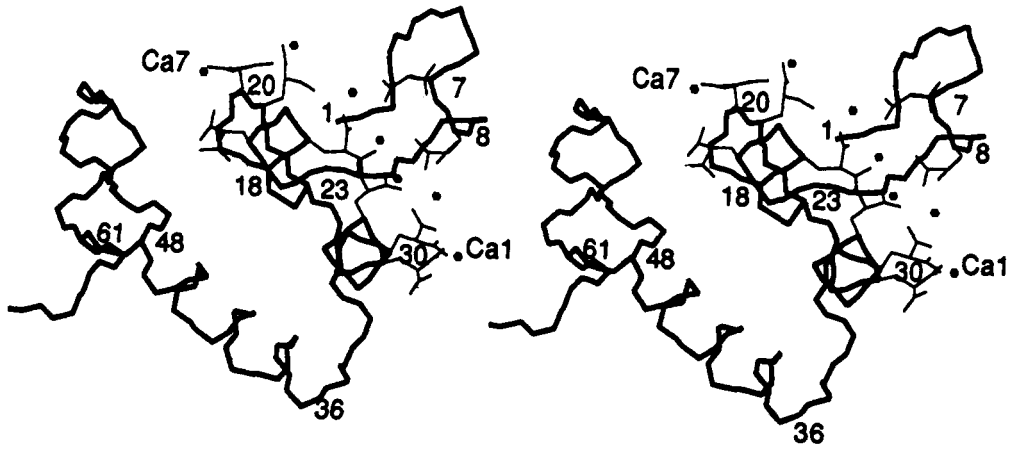

FIGURE 2: Stereoview of the CA, C, N structure of the Gla domain and trailing disulfide loop. Side chains of Gla residues also shown along with Ca^{2+} ion positions as dots; Ca^{2+} ions numbered sequentially 1–7.

was sin θ/λ dependent. The R factor converged at 0.171 with an average thermal parameter of 28 Å^2 and became insensitive to further reduction by systematic adjustment of refinement parameters. The carbohydrate of fragment 1 (5 kDa, 20% of the total structure) remained disordered throughout the refinement, similar to the apo-fragment 1 structure (Park & Tulinsky, 1986; Seshadri et al., 1991); in addition, no density was observed for the interkringle dodecapeptide C-terminal residues. The latter is most likely the result of the loss of five amino acids from the C-terminal during crystallization (Olsson et al., 1982; Soriano-Garcia et al., 1989), causing the remaining residues to be disordered. The final target parameters of the refinement and their rms values are listed in Table I along with other statistics pertinent to the final structure. An examination of the R factor as a function of scattering angle suggests a coordinate error (Luzzati, 1952) of about 0.20–0.25 Å; this value is most likely much less for Ca^{2+} ion positions because of their higher electron density peak heights. The occupancies of the Ca^{2+} ions refined to unity for Ca-1 through Ca-5 and 0.90 and 0.89 for Ca-6 and Ca-7, respectively; the B values of the former ranged from 23 to 28 Å^2, while the latter were 35 and 26 Å^2. The last two Ca^{2+} ions might not be quite fully occupied. The same applies to the Sr-fragment 1 structure (Sr-6 = 0.63, Sr-7 = 0.62) that is remarkably similar to that of Ca-fragment 1 (unpublished results of this laboratory).

Results and Discussion

The Gla Domain: General

Although the folding of the polypeptide chain of the Gla domain is fairly simple, it produces a complex stereochemical tertiary structure for the side chains of more than half of the Gla residues. The N-terminal α-helix (Ser36–Ala47) of apo-fragment 1 (Park & Tulinsky, 1986; Tulinsky et al., 1988; Seshadri et al., 1991) is preceded by a reverse-like turn and then two more turns of helix (Arg25–Ala31) which run antiparallel and at about 45° to the longer helix (Figure 2). The shorter helix connects to the conserved Cys18–23 disulfide loop of the Gla domain through Ser24. The hexapeptide loop is followed by another turn of the helix (Leu14–Gla17), and since the tight disulfide loop itself resembles a helical turn, together, the loop and Leu14–Gla17 approximate two turns of helix (Figure 2). The N-terminal 12 or so residues correspond to an ω-loop-like structure but with residues Gly4-Phe5 associated with poorly defined electron density. A ribbon drawing of the folding highlighting the secondary structural elements of the Gla domain and its accompanying tetradecapeptide disulfide loop is shown in Figure 3.

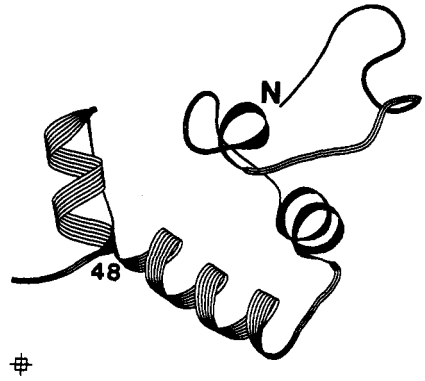

FIGURE 3: Ribbon drawing of the folding of the Gla domain and trailing disulfide loop. Disulfide bonds are not shown; the N-terminal and Cys48 are designated.

Table II: Accessible Area (AA) of Ca^{2+} Ions, Gla, and Other Pertinent Residues

			%AA[b]				
Ca^{2+}	AA (Å^2)[a]	%AA	Gla	OE1	OE2	OE3	OE4
1	41.4	32	7	**0**	**2**	21	11
2	11.7	9	8	63	**9**	**0**	**6**
3	2.0	2	15	69	64	(4)	(**0**)
4	0.0	0	17	**0**	**0**	(**0**)	**0**
5	9.1	7	20	34	**1**	**7**	(**45**)
6	43.6	33	21	47	**54**	**0**	(**1**)
7	53.0	40	26	28	**9**	**17**	90
			27	**0**	**3**	12	(**0**)
			30	**27**	78	**4**	**0**
Ala1N	0.0	0					
Cys18S	0.0	0					
Cys23S	0.0	0					
Phe41[c]	18.0	9					
Trp42[c]	61.4	25					
Tyr45[c]	14.1	6					

[a] Free Ca^{2+} ion = 131 Å^2. [b] Free Gla carboxylate oxygen = 47.5 Å^2; boldface, involved in a Ca–O interaction; parentheses, involved in an ion pair interaction with Ala1, Arg16, or Arg55. [c] Side chain only.

Five Ca^{2+} ions are chelated between Gla7–Gla8, Gla17, Gla26–Gla27, and Gla30 (no density was observed for the side chain of Gla33) in a polymeric arrangement not unlike those described in calcium malonate complexes [see Yokomori and Hodgson (1988) and references therein]. The latter four observed Gla residues form an internal carboxylate surface which, along with a smaller one of Gla7–Gla8, surround the five Ca^{2+} ions (Figure 2) and render four of them (Ca-2 to Ca-5) inaccessible to solvent (Table II). The distances between Ca^{2+} ions in the polymeric arrangement are 1–2 = 4.4 Å, 2–3 = 4.0 Å, 3–4 = 3.8 Å, and 4–5 = 3.8 Å, and, except

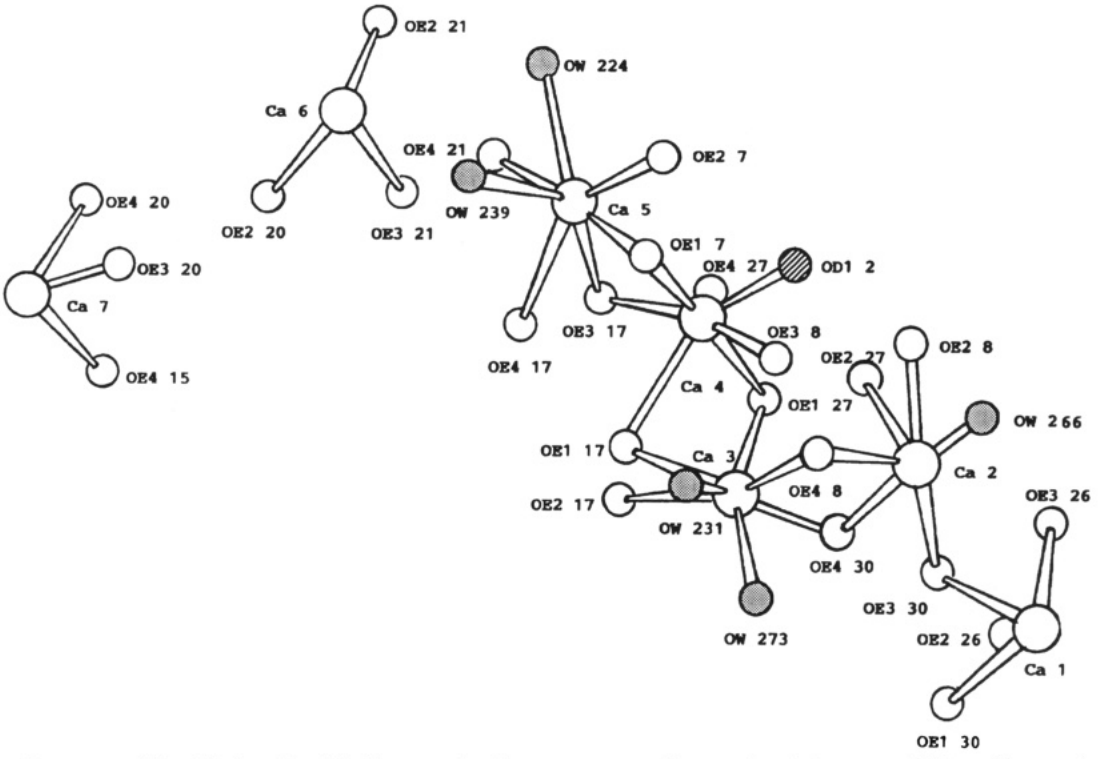

FIGURE 4: Ca–O structure of the Gla domain of Ca-fragment 1. Oxygen atoms are from carboxylate groups of Gla residues, water molecules (speckled), and OD1 of Asn2 (cross-hatched); oxygen numbering gives the atom number first followed by the residue number.

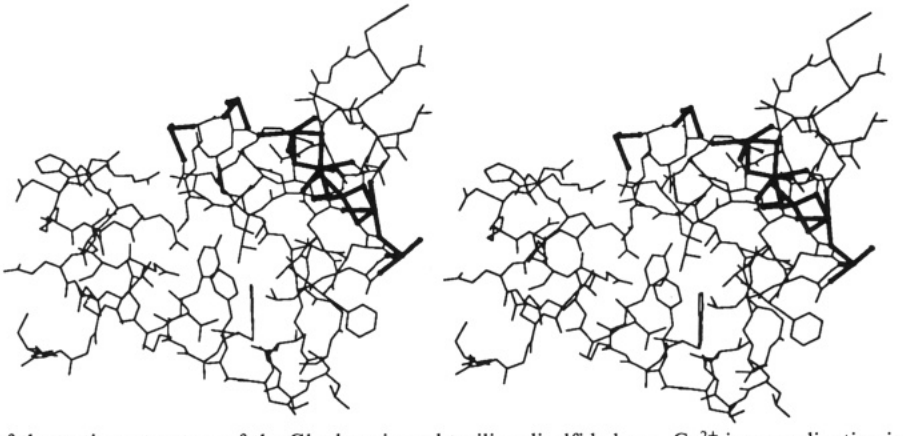

FIGURE 5: Stereoview of the tertiary structure of the Gla domain and trailing disulfide loop. Ca^{2+} ion coordination is indicated in bold; the orientation is as in Figure 2.

for Ca-2, they are in a linear array along an arc buried among the six Gla residues. Thus, Ca^{2+} ions 2–5 are practically in contact with one another, with each one in contact with three or more different Gla residues.

The Gla residues 15, 20, and 21 appear to form a separate, looser Ca^{2+} ion cluster involving the hexapeptide disulfide loop of the Gla domain (Figure 2). The last Ca^{2+} ion of the linear array (Ca-5) is 5.4 Å from Ca-6 of this cluster, while Ca-6 bridges Gla20–Gla21 of the loop, and Ca-7 is between Gla15 and Gla20. The latter two Ca^{2+} ions are fairly exposed to solvent (Table II), and the separation between these Ca^{2+} ions is also considerably larger at 8.5 Å. Thus, seven Ca^{2+} ions interact with 24 oxygen atoms of 16 of 18 carboxylate groups of the nine ordered Gla residues of the domain (Table II), completely burying four of the Ca^{2+} ions.

The Calcium Gla-Carboxylate Structure

Of the 36 carboxylate oxygen atoms observed in the Gla domain, 24 make direct bonds with Ca^{2+} ions (Figure 4, Table III), with Gla17 and Gla27 being completely buried within the domain. Moreover, seven of the oxygen atoms are involved in μ-oxo-like bonds bridging two Ca^{2+} ions (Einspahr et al., 1986), and one of the Ca^{2+} ions (Ca-4) coordinates OD1 of Asn2 (Figure 4). The manner in which this complex Ca–O structure is incorporated into the folded Gla domain is shown in Figure 5, and a typical electron density distribution characteristic of Ca^{2+} ion–Gla interactions is presented in Figure 6. Such cyclic distributions fused to one another were imperfect in the early stages of the work and confusing and difficult to interpret.

The coordination around the Ca^{2+} ions (Table III) does not correspond well to any of the idealized polyhedra, although Ca-1 approximates a tetrahedron, Ca-3 a capped octahedron, Ca-4 a 4:3 geometry, and Ca-5 a distorted pentagonal bipyramid (Figure 4). Nine unidentate interactions by carboxylate oxygens dominate the Ca–O interactions. Malonate or chelate coordination (Zell et al., 1985) utilizing both carboxylates of a Gla residue occurs six times, while bidentate coordination through a given carboxylate is least prevalent with only five carboxylates displaying this mode of binding.

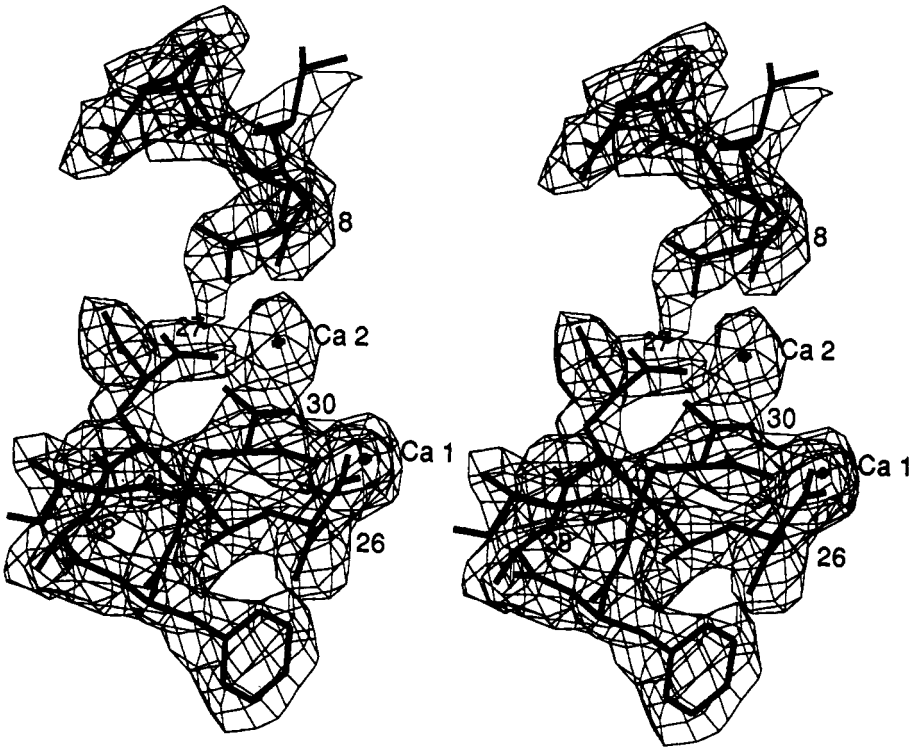

FIGURE 6: Stereoview of $(2|F_o| - |F_c|)$ map in the vicinity of Ca-1 and Ca-2. Gla residues are numbered and contoured at the 1σ level.

However, the total number of oxygens involved in each of these coordination modes is comparable at 9, 12, and 10, respectively. The first five Ca^{2+} ions are further linked together with a μ-oxo bond between Ca-1 and Ca-2 and di-μ-oxo bonds between Ca-2 and Ca-3, Ca-3 and Ca-4, and Ca-4 and Ca-5 (Figure 4). The di-μ-oxo bonds also display generally smaller interatomic distances. The remaining two Ca^{2+} ions (Ca-6, Ca-7) have distorted pyramidal coordination and are relatively exposed to solvent (Table II). Somewhat surprisingly, they do not appear to coordinate any water molecules of solvent whereas three of the other Ca^{2+} ions incorporate at least one water in the coordination sphere, except Ca-4, which is completely buried near the center of the Gla domain (Table II, Figure 4) and Ca-1, which, like Ca-6 and Ca-7, is also relatively exposed (Table II). It is of particular note that the penta-Ca^{2+} ion array is surrounded by 18 carboxylate oxygen atoms so that, on the average, the cluster is essentially electrically neutral, while Ca-6 and Ca-7 possess a small net positive charge of about $^1/_2$ each, raising the possibility that this cluster might be utilized in a binding interaction with negative charges of phospholipid.

Of the 12 carboxylate oxygen atoms not involved in Ca^{2+} ion interactions, 4–5 are inaccessible from the solvent while only Gla21OE2 of the bonded oxygens is relatively exposed (Table II). This leaves only about seven Gla carboxylate oxygen atoms accessible for phospholipid binding through bridging Ca^{2+} ions. Of these, four correspond to a pair of carboxylate groups (on Gla15 and Gla21) which are 13 Å apart, while the other three are relatively isolated from one another. Thus, except for the Ca-6, Ca-7 Gla-residue cluster, which carries a partial positive charge, only Gla 15 and Gla 21 appear to be reasonably situated to enter into a further Ca^{2+} ion–phospholipid coordination interaction, unless such interactions can transpire with low coordination numbers. However, Gla20–Gla21 may participate indirectly if the Ca-6, Ca-7 positive cluster interacts with negative head groups of the surface.

The Ca–O distances to Gla residues range from about 2.0 to 3.1 Å and correspond well with Ca–O distances observed in other proteins (Strynadka & James, 1989) and carboxylic acid–calcium salts (Einspahr & Bugg, 1981); the 6- and 7-fold coordination of the Ca^{2+} ions correspond likewise. The Ca-4–Gla17OE1 distance of 3.1 Å lies outside the range somewhat but might be part of an unsymmetrical μ-oxo interaction. A similar, weaker interaction has also been observed with calcium benzylmalonic acid (Yokomori & Hodgson, 1988). The lone Ca–O interaction not involving a Gla residue (Asn2OD1) is at the short end of the distance range, while the six coordinating water molecules have distances from 2.4 to 3.2 Å but are less reliably determined.

The aggregation of the first five Ca^{2+} ions of the Gla domain into the polymeric arrangement is additionally reinforced by the presence of one single μ-oxo bond and three di-μ-oxo bridges (Figure 4). The single μ-oxo bond and one between Ca-2 and Ca-3 arise from a bidentate interaction of a single carboxylate group of Gla30, while one μ-oxo bond in each of the other di-μ-oxo bridges is from a malonate interaction of Gla17 involving Ca-3, Ca-4, and Ca-4, Ca-5 (Figure 4). The bond angles and other pertinent parameters of the bridges are presented in Table S-1 in the supplementary material (see paragraph at end of paper regarding supplementary material) from which it will be seen that the di-μ-oxo bridge between Ca-2 and Ca-3 produces a planar array while the other two have a pucker with the one between Ca-3 and Ca-4 being fairly symmetrical.

From the complexity and the high degree of sophisticated organization displayed among the Gla residues and the Ca^{2+} ions, it is clear that the latter most likely orchestrate and serve as a nucleus for the folding transition leading to the phospholipid binding conformation displayed by Ca-fragment 1, Ca-prothrombin, and other Gla domain containing proteins. Consequently, the disorder of the domain that was observed in the apo-fragment 1 structure (Park & Tulinsky, 1986; Tulinsky et al., 1988; Seshadri et al., 1991) must be the result of an unfolded polypeptide chain and not that of a disorder of a folded structure. Moreover, Ca-2 to Ca-5 probably

Table III: Ca^{2+} Ion Coordination and Ca–O Distances of the Gla Domain

Ca^{2+}	CN[a]	overall type	ligand[b] (residue oxygen)	d (Å)	specific type
1	4	$(mal)_2$	26O2	2.4	malonate
			26O3	2.5	
			30O1	2.4	malonate
			30O3[c]	2.5	
2	6	(uni)(bi)(mal)(H_2O)	8O2	2.7	malonate
			8O4[c]	2.7	
			27O2	2.8	unidentate
			30O3[c]	2.4	bidentate
			30O4[c]	2.5	
			O_w266	2.7	
3	7	$(uni)_3(bi)(H_2O)_2$	8O4[c]	2.4	unidentate
			17O1[c]	2.5	bidentate
			17O2	2.7	
			27O1[c]	2.7	unidentate
			30O4[c]	2.6	unidentate
			O_w231	2.4	
			O_w273	2.4	
4	7	$(uni)_2(mal)_2$OD1	7O1[c]	2.8	unidentate
			8O3	2.7	unidentate
			17O1[c]	3.1	malonate
			17O3[c]	2.0	
			27O1[c]	2.6	malonate
			27O4	2.6	
			Asn2OD1	2.1	
5	7	$(uni)(bi)_2(H_2O)_2$	7O1[c]	2.5	bidentate
			7O2	2.5	
			17O3[c]	2.5	bidentate
			17O4	2.9	
			21O4	2.8	unidentate
			O_w224	3.2	
			O_w239	3.1	
6	3	(uni)(mal)	20O2	2.6	unidentate
			21O2	2.7	malonate
			21O3	2.4	
7	3	(uni)(bi)	15O4	2.8	unidentate
			20O3	2.4	bidentate
			20O4	2.8	

[a] CN is the coordination number. [b] OE of Gla residues is listed as O for simplicity. [c] Participates in the μ-oxo bond between two Ca^{2+} ions.

correspond to the 3–4 Ca^{2+} ions associated with the tight, cooperative Ca^{2+} ion binding sites previously identified in solution studies (Nelsestuen et al., 1975; Nelsestuen, 1976, 1984; Bajaj et al., 1975; Prendergast & Mann, 1977; Bloom & Mann, 1978; Deerfield et al., 1987) which ultimately lead to the native membrane binding structure. The cooperativity is consistent and correlates well with the complexity of the Ca^{2+} ion interaction resulting from the folding transition.

The orientations of the carboxylic acid groups of the Gla residues are summarized in Table S-2 (supplementary material), which lists the dihedral angles between them. The two carboxylate groups of a Gla residue are generally staggered with respect to each other since a coplanar arrangement leads to a very close van der Waals contact between oxygens of different carboxylates and consequently like charges. Only Gla15, Gla20, and Gla26 have small dihedral angles. In the case of Gla15, it makes a hydrogen bonding ion pair with Arg55 and a unidentate contact with Ca-7, while, with Gla20, two carboxylates bridge Ca-6 and Ca-7 (Figure 4) and, with Gla26, the smaller angle achieves a malonate-type interaction (Table III). However, small dihedral angles have even occasionally been observed in much simpler arrangements such as in calcium benzylmalonic acid (Yokomori & Hodgson, 1988). Except for these three residues of the Gla domain, the average dihedral angle between Gla carboxylates is 76°.

From the three-dimensional structure of the Gla domain, it appears that the presence of Gla in preference to glutamic acid in the phospholipid binding domain is related to the ability of Gla to provide more carboxylate groups to form connected polymeric arrays linking a number of Ca^{2+} ions with each other. It is indeed impressive that this tenet was originally inferred and suggested from small structure crystallographic studies of calcium malonate and malonate derivatives (Yokomori & Hodgson, 1988). The penchant for Ca^{2+} ion association and its flexibility in adapting to different and distorted coordination geometries, along with the abundant concerted supply of carboxylate groups from Gla side chains, are clearly the underlying principles which dictate the folding of the Gla domain. In contrast, Mg^{2+} ion complexes of malonates, polyethers, or peptides (Curry et al., 1985) are generally strictly six-coordinate, octahedral, and monomeric and due to the small size of the Mg^{2+} ion possess short Mg–O distances of about 2.0–2.1 Å (Spiro, 1983). Thus, Mg^{2+} ions do not bind cooperatively (Deerfield et al., 1987) in the high-affinity Ca^{2+} ion sites in the same manner as Ca^{2+} ions, most likely because of their less forgiving nature. The result is to produce a different Gla domain conformation which affects intrinsic fluorescence but does not bind phospholipid. Intermediate hybrid effects must pertain to other cations which can lead to a phospholipid complex but which is different from that resulting from Ca^{2+} or Sr^{2+} ions (Nelsestuen et al., 1976).

It has been reported that there is also a metal ion binding site in the kringle region of fragment 1 (Lundblad, 1988; Welsch & Nelsestuen, 1988b). This site is in the vicinity of carbohydrate-carrying Asn101 because Ca^{2+} and Mg^{2+} ion protect ND2 of Asn101 from acetylation. Moreover, acetylation of this site causes a loss of metal ion induced fluorescence change. Examination of electron density maps of this region during and at the end of refinement did not reveal any density which could reasonably be expected to correspond to Ca^{2+} ions. An electron density peak is located 3.2 Å from Asn101ND2 which has been interpreted to be a water molecule (O284) with an occupancy of 0.6 (B = 31 Å^2) but could conceivably correspond to a very partially occupied Ca^{2+} ion (~0.3). However, it has no semblance of other coordination and truly appears to simply be a hydrogen-bonded water molecule of solvation. The next positionally closest water peak to Asn101 is 4.1 Å away (O221, occupancy = 0.8, B = 22 Å^2). Although it is possible that the conformational change accompanying Ca^{2+} ion binding indirectly affects the accessibility of Asn101ND2, the effect must then be somewhat reversible since acetylation affects Ca^{2+} ion binding as evidenced by the loss of fluorescence quenching upon derivatization.

The Gla Residues

Modification of Gla7, Gla8, and Gla33 of fragment 1 (Zapata et al., 1987) reduces the Ca^{2+} ion binding affinity by about 10-fold, and the resulting protein loses its Ca^{2+} ion dependent membrane binding ability as well. From the structure of the Gla domain and the disorder of the Gla33 side chain, the Gla33 modification would seem to be unimportant. However, Gla7 and Gla8 are involved in seven Ca–O interactions with Ca-2 to Ca-5 (Table III, Figure 4), so it is not surprising that their conversion to γ-methyleneglutamyl residues results in marked effects abolishing membrane binding activity. The corresponding Gla residues of protein C have also been converted to aspartate using recombinant technology (Zhang & Castellino, 1990). When this mutant protein is activated, its ability to inactivate factor VIII is less than 5% of that of the recombinant wild-type. Since Ca^{2+} ions are required for the inactivation process, Gla6 and Gla7 of protein C are clearly vital for the full expression of anticoagulant activity of activated protein C. The Gla residues of the hex-

apeptide disulfide loop of protein C were also converted to aspartates using similar methods (Zhang & Castellino, 1991). These studies showed that Gla19 and Gla20 of protein C affect Ca^{2+} ion properties of a Gla domain independent effect which influences kinetic properties of protein C activation and are of very significant importance to the factor VIII anticoagulant properties of the enzyme. In Ca-fragment 1, there is (a) an interaction between Gla15, Gla20, and Ca-7, (b) a Gla20 bridge between Ca-6 and Ca-7 (Figure 4), and (c) a shared salt bridge between Arg55 of the trailing disulfide loop and Gla15 and Gla20. The latter interaction appears to be important in supporting the folded structure of the Gla domain (see *Gla Domain–Disulfide Loop Interaction* below). The disruption of a comparable interaction in protein C between the Gla domain and an EGF module involving the same Gla residue (Gla19) could be responsible for the diminished Ca^{2+} ion dependent behavior observed for the mutant protein (Zhang & Castellino, 1991).

All Gla domain proteins except prothrombin contain a Gla residue at position 36 (or equivalent); factors IX and X and protein Z additionally have a Gla at 40 (Tulinsky et al., 1988). Position 36 is located at the carboxy end of the reverse turn between the two- and three-turn helices of the Gla domain (Figure 2), while residue 40 is one helical turn removed from position 36. A Gla at 36 alone would appear to have little functional significance, unless it interacts with a trailing disulfide or EGF domain, since the side group simply extends out into the solvent in Ca-fragment 1. However, Gla36 with an additional Gla at 40 could conceivably produce another Ca^{2+} ion binding site between the two residues. This site would be in the interdomain space between the Gla and kringle domains in Ca-fragment 1 (Soriano-Garcia et al., 1989) and cannot be utilized in this molecule because of (a) insufficient space to accommodate the Gla residues and (b) insufficient space to coordinate a Ca^{2+} ion robustly (for more about this region, see below).

The Gla Domain: Specifics

Other notable aspects of the folding and the tertiary structure of the Gla domain are (a) the disulfide of the conserved loop (Cys18–Cys23) is buried in the conserved aromatic cluster (Phe41–Trp42, Tyr45) of the domain generated by a turn of the longer helix (Table S-3, supplementary material); (b) the amino terminus of Ala1 participates in three ion pair interactions with different Gla residues involving hydrogen bonding (Table IV), rendering the quaternary amino group inaccessible to solvent; (c) the Gla domain and its trailing tetradecapeptide disulfide loop are linked by two salt bridges and a number of other contacts producing a domain-like structure (Table S-4, supplementary material); (d) the Gla domain is relatively flat (~18 Å) like that of its accompanying kringle and assumes a triangular discoid shape; (e) unlike its interaction with the trailing disulfide loop, the Gla domain and the kringle are not intimately miscible at their contact region and appear to be distinct physical entities separated by a long, narrow, definite gap occupied with solvent water molecules; and (f) there are 20 well-defined intramolecular hydrogen bonds in the Gla domain and five in its trailing disulfide loop, which include six in α-helices and seven in ion pair interactions (Table IV).

(*a*) *Fluorescence Quenching.* In the presence of Ca^{2+} ions at equilibrium and at neutral pH, the intrinsic fluorescence of fragment 1 is quenched by about 40% (Nelsestuen, 1976; Prendergast & Mann, 1977); that of dissolved crystalline Ca-fragment 1 is comparable (Soriano-Garcia et al., 1989) so that the present structure must be considered pertinent. In

Table IV: Intramolecular Hydrogen Bonds in the Gla Domain of Fragment 1[a]

donor	acceptor	distance (Å) D···A	angle (deg) DHA	angle (deg) CAH	comments
Ala1N	Gla17OE3	2.7	109	131	ion pair
Ala1N	Gla21OE4	2.9	137	139	ion pair
Ala1N	Gla27OE4	3.0	133	129	ion pair
Lys3N	Gla7OE2	2.3	151	130	
Arg16NH2	Gla17OE4	3.2	144	114	ion pair
Cys18N	Leu14O	3.0	152	118	α-helix
Leu19N	Leu14O	3.0	144	152	
Cys23N	Try45OH	2.8	153	155	
Arg25NH1	Asp39OD2	2.2	125	167	ion pair
Gla30N	Gla26O	2.8	157	130	α-helix
Leu32N	Phe29O	2.9	159	121	
Gla33N	Phe29O	3.0	172	174	
Ala37N	Ser34OG	2.9	136	118	
Thr38OG1	Ser34O	2.7	151	143	
Asp39N	Leu35O	2.8	156	151	α-helix
Phe41N	Ala37O	2.9	152	126	α-helix
Trp42N	Thr38O	2.5	141	141	α-helix
Lys44NZ	Leu62O	2.7	175	162	
Tyr45N	Phe41O	2.7	126	159	α-helix
Thr46OG1	Trp42O	2.7	168	143	
Ala51N	Cys48O	2.9	143	126	
Arg55NH1	Gla15OE3	2.2	157	121	ion pair
Arg55NH2	Leu19O	2.5	128	127	
Asn59N	Arg55O	2.9	155	121	
Asn59ND2	Arg55O	2.7	154	167	
other significant interactions					
Ala1N	Ca-4	3.8			
Ala1N	Ca-5	2.8			
Arg52NH1	Glu49OE2	4.0	144	132	possible ion pair

[a] D = donor, A = acceptor, and H = hydrogen. Hydrogen-bond criteria: distance <3.0 Å, DHA angle >125°, and CAH angle >118°.

factor X, the change was found to result from perturbations in the environment of the lone tryptophane residue of the Gla domain (Persson et al., 1991). The fluorescence process is biphasic in fragment 1 and proceeds with an initial fast component of 25% (<1 s) followed by a relative slow one (>10 min) (Nelsestuen, 1976; Marsh et al., 1979). Moreover, the phospholipid binding behavior parallels the fluorescence quenching in that about 25% of fragment 1 binds Ca^{2+} ion immediately upon addition, but thereafter the binding follows the slow quenching process. To account for the phenomenon, it was proposed that two species of fragment 1 exist at equilibrium, containing a smaller amount of cis and a larger amount of trans component of proline and that a slow interconversion from *trans*-to *cis*-proline produces the observed quenching pattern (Marsh et al., 1979).

An examination of the structure of the Gla domain of Ca-fragment 1 reveals that the disulfide of Cys18–Cys23 of the conserved disulfide loop interacts with the conserved aromatic cluster of Phe41, Trp42, and Tyr45 (Figure 7 and Table S-3, supplementary material) and further, that both are covered on one side by the side chains of Leu14, Leu19, Leu32, Leu58, Leu62, and Ala28 (Table II and Figure 5). This is in agreement with the blue-shift in fluorescence of factor X upon Ca^{2+} ion binding, implying a more hydrophobic environment around the tryptophane residue (Persson et al., 1991). The close proximity of the disulfide to the indole of Trp 42 causes the χ_1 and χ_2 angles of the side group to change by 96° and 42°, respectively, compared to apo-fragment 1 (Figure 7). This reorientation is most likely the event responsible for the fluorescence quenching that accompanies the metal ion induced conformational change. In contrast to such a movement are Trp90 and Trp126 of the kringle, which are positionally the

FIGURE 7: Stereoview of the superposition of the Ser36–Ala47 helix of apo-fragment 1 on the Gla domain. The CA, C, N structure of the Gla domain is in bold; the aromatic cluster of both structures is shown.

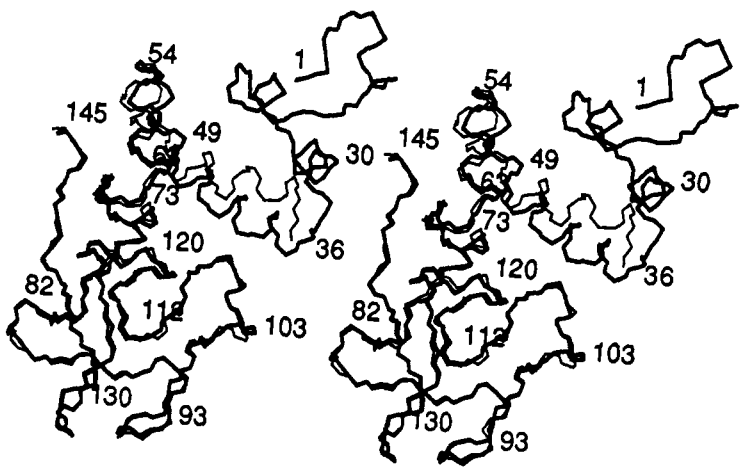

FIGURE 8: Stereoview of the superposition of the CA, C, N kringle structures of apo-fragment 1 and Ca-fragment 1. Ca-fragment 1 is in bold.

same in both the Ca-fragment 1 and fragment 1 structures. Precedence for a disulfide–π-electron interaction has already been set with the structure determination of a fluorescent probe ANS–α-chymotrypsin complex (Weber et al., 1979), where the naphthyl group of ANS binds at a single surface site and interacts with Cys1–Cys122. Reduction of the Cys18–Cys23 disulfide of the Gla domain (Schwalbe et al., 1989) or the lack of Tyr45 in a proteolytic fragment thereof decreases Ca^{2+} ion binding affinity (Pollock et al., 1988; Schwalbe et al., 1989) and abolishes or alters membrane binding in a Ca^{2+} ion dependent manner. The dependence on Tyr45 further indicates that the three-residue aromatic cluster is an important feature of the phospholipid binding structure. Disruption of the disulfide loop by conversion of Cys22 of protein C to serine also reduces Ca^{2+} ion dependent anticoagulant activity to 1% of that displayed by wild-type recombinant protein C (Zhang & Castellino, 1991).

In the absence of Ca^{2+} ion, the equilibrium cis/trans conformers of fragment 1 were proposed to be those involving Pro22 (Marsh et al., 1979). However, the conformation of Pro22 is trans in the structure of Ca-fragment 1, not in agreement with the proposed isomerization. A more likely candidate for the process is Pro54 of the tetradecapeptide disulfide loop, which is in a cis conformation in Ca-fragment 1 but is trans in apo-fragment 1 (Seshadri et al., 1991); moreover, the electron density in this region is not as well-defined in the latter structure, which is consistent with it being due to an equilibrium mixture of conformers. Furthermore, the cis conformation of Pro54 in the tetradecapeptide loop might help align Arg55 so that is can form important ion pair interactions with Gla15 and Gla20 of the Gla domain which lead to a close association between these two structural motifs (Table IV, Table S-4 supplementary material, and Figure 5). Another *cis*-proline occurs in the structure in the kringle domain (Pro95), but it has been observed in other kringles also (Seshadri et al., 1991; Mulichak et al., 1991).

In addition to the folding transition of the N-terminal 35 residues of fragment 1 upon Ca^{2+} binding, the Gla domain helix of apo-fragment 1 (Ser36–Ala47) undergoes a 30° rigid body pivot in the vicinity of Cys48–Cys59 in Ca-fragment 1 (Soriano-Garcia et al., 1989) which makes it encroach upon the kringle domain (Figure 8). The gap between the domains is narrowed from about 9 Å in the apo-structure to about 5 Å in Ca-fragment 1. However, the two domains remain distinctly separate, and the space between them is generally occupied by water molecules in both structures (Seshadri et al., 1991).

(*b*) *N-Terminal Ala1*. The N-terminus of the Gla domain is embedded in the folded structure and is completely buried. It makes ion pair interactions with Gla17, Gla21, and Gla27 involving hydrogen bonds (Figures 2 and 5, Table IV), and it has no exposed area to surface solvent (Table II). Moreover,

it may also be interacting with Ca-4 and Ca-5 (Table IV), all of which agrees with the observation that Ala1 is protected from acetylation by Ca^{2+} ions (Welsch & Nelsestuen, 1988a). The presence of Ca^{2+} ions has no effect on the fluorescence of the Gly12–Lys44 fragment of prothrombin, which contains eight Gla residues and does not bind to phospholipid (Nelsestuen & Suttie, 1973). Once again, this suggests the importance of Gla7 and Gla8 and/or the N-terminal region for the conformational change. From the structure of the Gla domain, it would seem that both are crucial for producing the correct folding in that the Gla residues participate in the high-affinity, cooperative sites, while burying the N-terminal might be more important in finalizing the details of the phospholipid binding conformation. The fact that Mg^{2+} ions do not protect against acetylation of the N-terminus (Welsch & Nelsestuen, 1988a) suggests that Mg^{2+} ion binding to the nonspecific metal ion binding sites does not lead to a conformation which buries Ala1 and thus also does not achieve a membrane binding state. The only known modification of the N-terminus which does not remove membrane binding ability is trinitrophenylation. Since such a bulky group cannot be accommodated in the space around the amino terminus in the underivatized structure, an alternate structure must form in which the N-terminal region still approximates the native case.

(*c*) *Gla Domain–Disulfide Loop Interaction.* The Gla domain of Ca-fragment 1 interacts and associates intimately with its trailing disulfide loop, which consists of an extended chain (Cys48–Arg55) and two turns of α-helix (Glu56–Glu63) so that the two motifs appear to form a three-dimensional structural unit which could easily be thought of as three-dimensional structural domain (Figure 5). The three turn α-helix of the Gla domain and the disulfide loop are approximately coplanar and about 100° apart and form an underlying foundation upon which the remainder of the triangular Gla domain discoid (Ala1–Leu35) anchors (Figure 5). The helix is probably one turn longer in Gla domains followed by an EGF domain (Tulinsky et al., 1988; Soriano-Garcia et al., 1989) so that the longer helix might serve a similar function with the extra helical turn assisting in better supporting a larger growth factor motif. This is in agreement with the observation that the bare Gla domain of prothrombin appears to be unable to assume a native conformation in the presence of Ca^{2+} ion unless it is linked to the disulfide loop and the first kringle (Pollock et al., 1988). The isolated Gla domain of factor X also has a lower affinity for Ca^{2+} ions compared with a Gla domain linked to the first EGF unit; moreover, the Gla domain affects the affinity of Ca^{2+} binding of the Gla-independent site on the EGF domain of factor X, both suggesting a stabilizing interaction between the two domains (Persson et al., 1991) which influences the metal ion binding sites. This is also in agreement with the proposal that the disulfide loop functions in producing high-affinity Ca^{2+} ion binding (Schwalbe et al., 1989), but clearly it must do so in an indirect manner.

The Gla domain and the disulfide loop of fragment 1 are held together through a surprisingly small number of interactions between Gla15, Leu19, and Gla20 of the former and only Arg55 of the latter (Table S-4, supplementary material). There is a total of 18 contacts less than 4.0 Å, mostly heteronuclear van der Waals interactions, of which 4–5 (25%) are salt bridges between the arginyl group of Arg55 and carboxylates of Gla15 and Gla20. These particular ion pairs might also be dependent on the *cis*-proline conformation of Pro54 mentioned earlier. In view of such a massive polar interaction to create this interface, the association between these motifs might be sensitive to ionic strength.

Kringle Domain

The kringle domains of Ca-fragment 1 and apo-fragment 1 have been compared by calculating the rotation matrix and translation vector which minimizes the squares of the differences of the CA, C, and N (Cys66–Cys144) coordinates between the two. The rms deviation of 237 atom pairs is 0.55 Å; removing 80 atoms with deviations $>1\sigma$ reduces the rms deviation to 0.33 Å. The deviations corresponding to other atoms or group classes based on this superposition are listed in Table S-5 (supplementary material). Although the fidelity of the folding between the two structures is, on the average, within expected error (Figure 8), many of the side chains appear to have undergone repositioning in Ca-fragment 1. Some of this is due to the different crystal packing environments of the two structures, while some of it appears to be related to the conformational shift of the Gla domain helix of apo-fragment 1 upon Ca^{2+} ion binding.

The immediate effect of the rigid body shift of the helix is on Val70–Arg75 of the kringle, which is in the hinge region (Leu62–Asn65) located adjacent to the gap between the Gla and kringle domains (Figure 8). The average rms change in main chain position here is 0.8 and 0.9 Å for side chains. These shifts, in turn, affect the first β-strand (Ser79–Thr81) of the β_1 structure of the kringle (Seshadri et al., 1991), which undergoes a lesser, but still significant, movement (0.7 Å, main chain; 0.7 Å, side chains). The Val70–Arg75 chain segment of the kringle is in a stacked position over the first inner loop (C in Figure 1) of the kringle (Tulinsky et al., 1988; Seshadri et al., 1991), and its movement appears to also propagate an adjustment to Asp119–Ser121 (0.8 Å, main chain; 1.3 Å, side chains). A similar effect occurs in a region about 15 Å away from the hinge at the far end of the helix near Leu36 (Figure 8): the main chain of Glu112–Asn113 moves by 1.1 Å and the side chains by 1.6 Å, causing a concomitant change between Glu99 and Thr104 (1.0 Å, main chain; 1.5 Å, side chains). The Glu112–Asn113 residues are in the second strand of the β_2 structure of the kringle (Seshadri et al., 1991), while Glu99–Thr104 is associated with Asn101, which carries one of the carbohydrates of fragment 1. The conformational change induced in the Asn101 region by the presence of Ca^{2+} ion is shown in Figure 9. This change must be somehow related to the Ca^{2+} ion protection of the acetylation of Asn101ND2 (Welsch & Nelsestuen, 1988a), but the manner in which it does is not clear. There is only one other significant structural change between Ca-fragment 1 and fragment 1, and it occurs near Ser92–Tyr94 (0.8 Å, main chain, 3.0 Å, side chains). This large change is due to a close crystal packing contact in the Ca-fragment 1 structure which does not exist in the tetragonal apo-fragment 1 crystals.

Electrostatic Potential of the Gla Domain

Since none of the preceding examination of the structure of the Gla domain revealed any obvious features to suggest the manner in which the Gla domain may bind to a phospholipid surface, the electrostatic potential of Ca-fragment 1 was calculated in two ways in an effort to gain insights which might be pertinent to the interaction. In the first, the computer program DELPHI (Biosym Technologies, Inc., San Diego, CA) was used for the calculation, which solves the Poisson–Boltzmann equation by finite differences (Gilson & Honig, 1987). The program employs the formal charges of ionized groups, the dielectric constant of the protein (water not included), and the dielectric constant of the surrounding solvent;

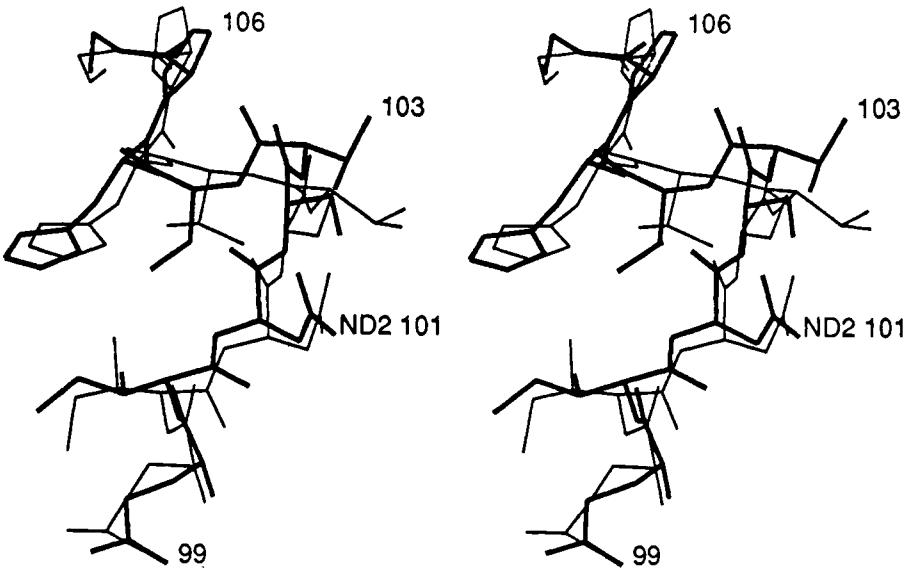

FIGURE 9: Stereoview of the superimposed structures of apo- and Ca-fragment 1 in the vicinity of carbohydrate carrying Asn101. Ca-fragment 1 is in bold.

the latter two were taken to be 2 and 80, respectively. An ionic strength can also be included in the calculation, but since it proved to be insensitive in the 150 mM region, it was neglected.

The other way in which the electrostatic potential was calculated (Nakamura & Nishida, 1987) involved the coordinate optimization minimizing the energy of a Gla residue with Gaussian 90 (STO-3G) and calculating the electrostatic potential of the optimized residue. The atomic charges of the Gla residue which reproduce the electrostatic potential were then obtained with AMBER, and other atomic charges of the Ca-fragment 1 were assigned AMBER parameters. Since both approaches gave essentially the same results, those produced by DELPHI will be described and discussed in what follows.

Prior to assigning the formal charges of ionized residues in DELPHI, the environment and the solvent distribution in the region of each charge was examined. As with other proteins (Wada & Nakamura, 1981), most of the charges were found to be paired and compensated in the form of salt bridges (Table IV). However, several charged side chains of the Gla domain and its trailing disulfide loop with well-defined electron density (Arg10, Lys44, Glu56, Glu60, Glu63) extended into solvent, two of which might be involved in a weak intermolecular ion pair interaction (Arg10–Glu63′, 4.9 Å). Moreover, the charge of Arg10 appears to be additionally compensated by a counterion,[2] and three water molecule dipoles surround Lys44. Although these residues appear to be more or less neutralized in the crystal structure, they were nonetheless assigned formal charges in the electrostatic potential calculation because the compensation could be an artifact of crystallization.[3] Thus, unit charges were assigned throughout the structure in a straightforward manner, except for guanidinium and carboxylate groups where fractional charges of $^1/_2$ were placed on equivalent atoms of the charged groups.

The electrostatic potential map of Ca-fragment 1 was examined at contour levels of ±1, ±5, and ±10kT/electron (kT = 0.6 kcal/mol). The 5kT energy contour corresponds to that of a hydrogen bond so that interactions at the level of this energy can be considered fairly significant. The most conspicuous features of the 1kT map of the Gla domain and the tetradecapeptide loop are (a) an electropositive surface that emanates from residues 1–21 of the Arg10, Arg16 discoid face extending 8–10 Å beyond the surface of the Gla domain, (b) the opposite face of the Gla domain is electronegative, making the domain a dipolar-faced discoid, (c) the trailing disulfide loop has a negative potential that also extends 8–10 Å from its surface, and (d) the kringle is very electropositive. The 5kT map was most notable in that (a) the electropositive potential of the Gla domain essentially disappears and is simply concentrated in the immediate vicinity of the Ca^{2+} ions, (b) the remainder of Gla domain is electronegative at this level, (c) the potential of the disulfide loop is only slightly diminished, and (d) the kringle remains highly positive. Interestingly, the 10kT map is only a slightly diminished version of the 5kT contoured potential. Thus, the three maps show that although the Gla domain possesses a positive component that extends well beyond its surface, it is generally weak and diffuse, diminishing to zero close to its surface.

From the 5- and 10kT maps, it is clear that the N-terminal two-thirds of the Gla domain is highly electronegative near its surface (within 2–3 Å) *even after compensating the charge of seven* Ca^{2+} *ions*, while the electrostatic potential of the Ca^{2+} ions only extends to their van der Waals radii at this level. Since the availability of free Gla residues for Ca^{2+} ion bridging interactions to a phospholipid surface is limited in number, the role of bridging Ca^{2+} ions might generally be unspecific in membrane binding and they may simply intercalate between an overall negative Gla domain and highly negative head groups of the membrane surface. Such a notion is in agreement with the observation that the first step of Gla domain–membrane binding of factor Xa is diffusion controlled (Krishnaswamy et al., 1988). Thereafter, movements or migration on the surface may lead to more definitive Gla–Ca^{2+}–PO_4 interactions. Experiments by us diffusing small organic phosphates into Ca-fragment 1 crystals to identify specific calcium–phosphate interactions failed to lead to such complexation in the crystalline state.

Although the positive electrostatic potential of the Gla domain is weak, it might nonetheless be of functional significance. Since it extends considerably beyond the surface, it is capable of interacting with a highly charged membrane surface at a distance. This, along with the dipolar nature of

[2] The electron density for W191 near Arg10 (2.6 Å) with an occupancy of 1.0 and B = 29 Å^2 has an exceptionally large volume and could be a partially occupied chloride ion.

[3] Not assigning charges to Arg10 and Lys44 had little significant effect on the overall electrostatic potential.

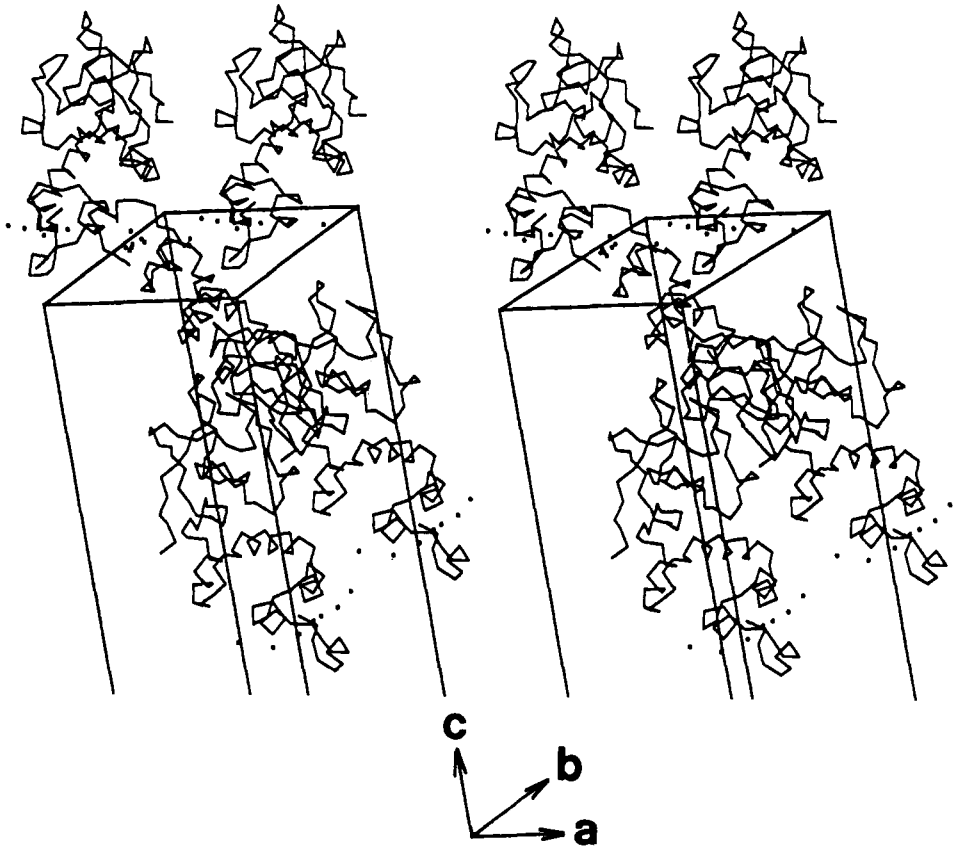

FIGURE 10: Stereoview of the packing of Ca-fragment 1 molecules in crystals. Ca-fragment 1 CA structure only: Ca^{2+} ions designated with dots form a zig-zagging channel in a plane approximately perpendicular to the *c*-axis.

the Gla domain discoid, could serve to orient the Gla domain as it approaches the surface. At a close approach to the surface, the negative potential of the Gla domain will dominate. The intercalation of bridging Ca^{2+} ions can alleviate this unfavorable interaction and can lead to phospholipid binding.

It is of note that the electrostatic potential of the accompanying disulfide loop of the Gla domain also has a relatively large negative component arising from Glu56, Glu60, and Glu63, while the kringle region is very electropositive due to 11 basic residues. Since kringle 2 of prothrombin has eight basic residues, it too is probably very electropositive so that the kringle–kringle interaction in fragment 1·2 and prothrombin might be a global dipolar one between the negative disulfide loop and a positive kringle 2 module.

Crystal Packing Interactions

The most striking feature of the crystal packing of Ca-fragment 1 is one involving the Ca^{2+} ions. The average distance between the Ca^{2+} ions which form a polymeric arrangement (Ca-1 to Ca-5) is 4.0 Å. In the crystal structure, Ca-1 of the asymmetric unit makes a 4.7-Å contact with Ca-7 of a symmetry-related neighboring molecule, while Ca-7 of the asymmetric unit makes an identical unitary contact with a different neighboring molecule (Figure 10). The seven Ca^{2+} ions of adjacent molecules thus interact in a head-to-tail fashion and extend infinitely through the crystal lattice producing a right-angle zig-zagging channel of Ca^{2+} ions surrounded by Gla domains (Figure 10).

An analysis of the intermolecular contacts of Ca-fragment 1 reveals that the majority of them are simply heteronuclear nonbonded van der Waals interactions. In all, there are 84 symmetry-related intermolecular contacts less than 4.0 Å for a given Ca-fragment 1 molecule. Residues Phe5–Leu6 of one molecule make 16 contacts with Ser36–Leu37 and Ala40 of the α-helix of the Gla domain of another molecule. The former are associated with the region of high negative electrostatic potential arising from the proximity of Gla residues, while the latter are associated with the residual positive charge around Arg 52. Thus, these intermolecular interactions appear to be reinforced by a global dipolar one similar to the intramolecular interaction between the disulfide loop and Gla domain.

The most important intermolecular contact between neighboring kringle motifs involves the turns of the second outer (B) and second inner (D) loops of one molecule (Figure 1) and the A,C loops and C-terminal of another, where Tyr94 alone makes 22 contacts less than 4.0 Å. Moreover, two of the contacts are good hydrogen bonds (Tyr94OH–Cys139O, 2.5 Å, and Val141N–Tyr94OH, 3.0 Å) and are the only intermolecular hydrogen bonds in the crystal structure. The resulting close intermolecular contact is also the reason for the large deviation between the structure of Ca-fragment 1 and apo-fragment 1 in this region (Ser92–Tyr94).

Acknowledgments

We thank Dr. Doug Rohrer of The Upjohn Company for discussions relating to the DELPHI electrostatic potential calculations and Dr. Haruki Nakamura of The Protein Engineering Institute, Osaka, Japan, for carrying out the self-consistent boundary electrostatic calculations.

Supplementary Material Available

Five tables, S-1 to S-5, further quantitating the Gla domain (5 pages). Ordering information is given on any current masthead page.

References

Bajaj, S. P., Butkowski, R. J., & Mann, K. G. (1975) *J. Biol. Chem. 250*, 2150–2156.

Bajaj, S. P., Nowak, T., & Castellino, F. J. (1976) *J. Biol. Chem. 251*, 6294–6299.
Bloom, J. W., & Mann, K. G. (1978) *Biochemistry 17*, 4430–4438.
Borowski, M., Furie, B. C., Bauminger, S., & Furie, B. (1986) *J. Biol. Chem. 261*, 14969–14975.
Brunger, A. T., Kuriyan, J., & Karplus, M. (1987) *Science 235*, 458–460.
Curry, M. E., Eggleston, D. S., & Hodgson, D. J. (1985) *J. Am. Chem. Soc. 107*, 8234–8238.
Deerfield, D. W., Olson, D. L., Berkowitz, P., Koehler, K. A., Pedersen, L. G., & Hiskey, R. G. (1987) *Biochem. Biophys. Res. Commun. 144*, 520–527.
Einspahr, H., & Bugg, C. E. (1981) *Acta Crystallogr. B37*, 1044–1052.
Einspahr, H., Parks, E. H., Suguna, K., & Subramanian, E. (1986) *J. Biol. Chem. 261*, 16518–16527.
Finzel, B. C. (1987) *J. Appl. Crystallogr. 20*, 53–55.
Furie, B. C., Mann, K. G., & Furie, B. (1976) *J. Biol. Chem. 251*, 3235–3241.
Gilson, M. K., & Honig, B. H. (1987) *Nature 330*, 84–86.
Gitel, S. N., Owen, W. G., Esmon, C. T., & Jackson, C. M. (1973) *Proc. Natl. Acad. Sci. U.S.A. 70*, 1344–1348.
Hendrickson, W. A. (1985) *Methods Enzymol. 115B*, 252–270.
Henriksen, R. A., & Jackson, C. M. (1975) *Arch. Biochem. Biophys. 170*, 149–159.
Krishnaswamy, S., Jones, K. C., & Mann, K. G. (1988) *J. Biol. Chem. 263*, 3823–3834.
Lundblad, R. L. (1988) *Biochem. Biophys. Res. Commun. 157*, 295–300.
Luzzati, V. (1952) *Acta Crystallogr. 5*, 802–810.
Marsh, H. C., Scott, M. E., Hiskey, R. G., & Koehler, K. A. (1979) *Biochem. J. 183*, 513–517.
Matthews, B. W. (1968) *J. Mol. Biol. 33*, 491–497.
Mulichak, A. M., Tulinsky, A., & Ravichandran, K. G. (1991) *Biochemistry 30*, 10576–10588.
Nakamura, H., & Nishida, S. (1987) *J. Phys. Soc. Jpn. 56*, 1609–1622.
Nelsestuen, G. L. (1976) *J. Biol. Chem. 251*, 5648–5656.
Nelsestuen, G. L. (1984) in *Metal Ions in Biological Systems*, (Sigel, H., Ed.) Vol. 17, pp 353–380, Marcel Dekker, Inc., New York.
Nelsestuen, G. L., & Suttie, J. W. (1973) *Proc. Natl. Acad. Sci. U.S.A. 70*, 3366–3370.
Nelsestuen, G. L., Zytkovicz, T. H., & Howard, J. B. (1974) *J. Biol. Chem. 249*, 6347–6350.
Nelsestuen, G. L., Broderius, M., Zytkovicz, T. H., & Howard, J. B. (1975) *Biochem. Biophys. Res. Commun. 65*, 233–240.
Nelsestuen, G. L., Broderius, M., & Martin, G. (1976) *J. Biol. Chem. 251*, 6886–6893.
Nelsestuen, G. L., Resnick, R. M., Wei, G. J., Pletcher, C. H., & Bloomfield, V. A. (1981) *Biochemistry 20*, 351–358.
North, A. C. T., Phillips, D. C., & Matthews, F. S. (1968) *Acta Crystallogr. 24A*, 351–359.
Olsson, G., Andersen, L., Lindqvist, O., Sjolin, L., Magnusson, S., Petersen, T. E., & Sottrup-Jensen, L. (1982) *FEBS Lett. 145*, 317–322.
Park, C. H., & Tulinsky, A. (1986) *Biochemistry 25*, 3977–3982.
Perrson, E., Bjork, I., & Stenflo, J. (1991) *J. Biol. Chem. 266*, 2444–2452.
Pollock, J. S., Shepard, A. J., Weber, D. J., Olson, D. L., Klappper, D. G., Pedersen, L. G., & Hiskey, R. G. (1988) *J. Biol. Chem. 263*, 14216–14223.
Prendergast, F. G., & Mann, K. G. (1977) *J. Biol. Chem. 252*, 840–850.
Schwalbe, R. A., Ryan, J., Stern, D. M., Kisiel, W., Dahlback, B., & Nelsestuen, G. L. (1989) *J. Biol. Chem. 264*, 20288–20296.
Seshadri, T. P., Tulinsky, A., Skrzypczak-Jankun, E., & Park, C. H. (1991) *J. Mol. Biol. 220*, 481–494.
Soriano-Garcia, M., Park, C. H., Tulinsky, A., Ravichandran, K. G., & Skrzypczak-Jankun, E. (1989) *Biochemistry 28*, 6805–6810.
Spiro, T. G. (1983) *Calcium in Biology*, pp 237–270, John Wiley & Sons, Inc., New York.
Stenflo, J., & Ganrot, P. O. (1973) *Biochem. Biophys. Res. Commun. 50*, 98–104.
Stenflo, J., Fernlund, P., Egan, W., & Roepstorff, P. (1974) *Proc. Natl. Acad. Sci. U.S.A. 71*, 2730–2733.
Strynadka, N. C. J., & James, M. N. G. (1989) *Annu. Rev. Biochem. 58*, 951–998.
Tulinsky, A., Vandlen, R. L., Morimoto, C. N., Mani, N. V., & Wright, L. H. (1973) *Biochemistry 12*, 4185–4192.
Tulinsky, A., Park, C. H., & Rydel, T. J. (1985) *J. Biol. Chem. 260*, 10771–10778.
Tulinsky, A., Park, C. H., & Skrzypczak-Jankun, E. (1988) *J. Mol. Biol. 203*, 885–901.
Wada, A., & Nakamura, H. (1981) *Nature 293*, 757–758.
Wang, B. C. (1985) *Methods Enzymol. 115B*, 90–112.
Weber, L. D., Tulinsky, A., Johnson, J. D., & El-Bayoumi, M. A. (1979) *Biochemistry 18*, 1297–1303.
Welsch, D. J., & Nelsestuen, G. L. (1988a) *Biochemistry 27*, 4939–4945.
Welsch, D. J., & Nelsestuen, G. L. (1988b) *Biochemistry 27*, 4946–4952.
Wyckoff, H. W., Doscher, M., Tsernoglou, D., Inagami, T., Johnson, L. N., Hardman, K. D., Allewell, N. M., Kelly, D. M., & Richards, F. M. (1967) *J. Mol. Biol. 27*, 563–578.
Yokomori, Y., & Hodgson, D. J. (1988) *Inorg. Chem. 27*, 2008–2011.
Zapata, G. A., Berkowitz, P., Noyes, C. M., & Hiskey, R. G. (1987) *Fed. Proc. 46*, 2230.
Zell, A., Einspahr, H., & Bugg, C. E. (1985) *Biochemistry 24*, 533–537.
Zhang, L., & Castellino, F. J. (1990) *Biochemistry 29*, 10828–10834.
Zhang, L., & Castellino, F. J. (1991) *Biochemistry 30*, 6696–6704.